Interference effects of two scalar boson propagators on the LHC search for the singlet fermion DM

P. Ko* and Jinmian Li†

School of Physics, Korea Institute for Advanced Study, Seoul 130-722, Korea

arXiv:1610.03997v2 [hep-ph] 13 Dec 2016

Abstract

A gauge invariant UV-completion for singlet fermion DM interacting with the standard model (SM) particles involves a new singlet scalar. Therefore the model contains two scalar mediators, mixtures of the SM Higgs boson and a singlet scalar boson. Collider phenomenology of the interference effect between these two scalar propagators is studied in this work. This interference effect can be either constructive or destructive in the DM production cross section depending on both singlet scalar and DM masses, and it will soften the final state jets in the full mass region. Applying the CMS mono-jet search to our model, we find the interference effect plays a very important role in the DM search sensitivity, and the DM production cross section of our model is more than one order of magnitude below the LHC sensitivity at current stage.

* pko@kias.re.kr
† jmli@kias.re.kr

I. INTRODUCTION

The existence of non-baryonic Dark Matter (DM) has been established by many astrophysical observations from gravitational effects [1]. However, the nature of DM and its interactions with other particles and among themselves remain unknown. Probing the DM signals at the hadron collider could elucidate the particle physics properties of DM without suffering from astrophysical uncertainties thus becomes one of the main object of the current and future LHC experiments as well as future colliders such as 100 TeV pp collider and high energy lepton colliders such as ILC or FCC-ee, CEPC. The strategy for DM search at colliders is rather simple: to look for events with large momentum unbalance that is produced by recoiling the DMs against energetic detector reconstructable objects such as jets.

The DM effective field theory (EFT) [2–4] which is supposed to be low energy approximation to a renormalizable theory for DM by integrating out the heavy particle that mediates the DM interaction has been widely used in early LHC analysis. The scalar $\times$ scalar operators describing the Dirac fermion DM χ interacting with Standard Model (SM) particles take the forms

$$\frac{1}{\Lambda^2}(\bar{\chi}\chi)(\bar{f}f), \quad \frac{1}{\Lambda^3}(\bar{\chi}\chi)\mathrm{Tr}(G^{\mu\nu}G_{\mu\nu}), \tag{1.1}$$

where the scale Λ has dimension of mass, f correspond to SM fermions and $G^{\mu\nu}$ is the gluon field. Then the limits on the DM relic density, DM direct/indirect detection and DM collider searches can be presented in terms of a common coefficient Λ and DM mass. However the EFT description might be useful only in the low energy phenomenology such as DM direct detection. At high energy scale such as at the LHC, unitarity shall be violated in general in the EFT approach [5–8]. Also thermal relic density or indirect detection would require extensions of operator basis involving other SM particles such as heavy quarks (c, b, t, etc.), the SM Higgs boson or electroweak gauge bosons.

In order to cure this problem of the DM EFT, simplified model frameworks have been proposed to undertake the DM searches at colliders [9–11]. The DM model Lagrangian with the minimal scalar mediator is defined as (Ref. [12] for example)

$$\mathcal{L} = \mathcal{L}_{\mathrm{SM}} + \frac{1}{2}(\partial_\mu\phi)^2 - \frac{1}{2}m_\phi^2\phi^2 + i\bar{\chi}\partial\!\!\!/\chi - m_\chi\bar{\chi}\chi - g_\chi\phi\bar{\chi}\chi - \sum_f g_v\frac{y_f}{\sqrt{2}}\phi\bar{f}f\ . \tag{1.2}$$

The model has 5 new parameters, DM mass m_χ, scalar mediator mass m_ϕ, DM-mediator coupling g_χ, SM-mediator coupling g_v and the mediator decay wdith Γ_ϕ, to which the collider search bounds can be applied. The collider phenomenology of simplified models with different mediator spins are also studied, in gluon gluon fusion production channel [13, 14] and in vector boson fusion production channel [15] if interactions between SM gauge bosons and the scalar are included. However, the simplified model Lagrangian (1.2) still has some problems, since the term $\frac{y_f}{\sqrt{2}}\phi\bar{f}f$ violates the SM gauge symmetry explicitly [16–18], because ϕ is a SM singlet scalar and $\bar{f}f$ is $SU(2)_L$ doublet. Therefore this simplified model may not be a suitable approximation/simplification of a UV-complete model for singlet fermion DM.

The simplest way to write down a renormalizable and gauge invariant UV completion for effective operator (1.1) is to introduce a singlet scalar s that interacts with SM particles by the mixing with the SM Higgs boson, where the singlet DM can be either a fermion [19] or a vector [20] particle. The LHC and the ILC searches for those minimal Higgs portal DM models with the full SM gauge symmetry are discussed in Ref. [16, 17, 21] and in Ref. [22],

respectively. And importance of the gauge invariance in DM collider phenomenology within other setups and/or contexts have also been studied in Ref. [23–27].

In this work, we continue the study of collider search for singlet fermion DM with scalar mediators within the gauge invariant and renormalizable Higgs portal DM model discussed in Ref. [19]. Comparing to previous studies [16, 17, 21], we consider the model with varying scalar decay width and resolved top quark in gluon gluon fusion production process. Moreover, the interference effects between two scalar propagators on both production cross sections and distributions of kinematic variables are discussed in detail. And their effects on the collider bounds for the singlet fermion DM searches at the LHC will be considered in terms of the CMS mono-jet/mono-V search.

This paper is organized as follows. A brief introduction on the gauge invariant UV completion of effective operator (1.1) is given in Sec. II in the framework of Higgs portal DM model. In Sec. III, taking the gluon-gluon fusion process as a representative example, we highlight the interference effects on both DM production cross section and final state distributions. More realistic applications to a CMS DM search including all dominant DM production processes are studied in Sec. IV. The results are summarized in Sec. V.

II. A GAUGE INVARIANT MODEL FOR SINGLET FERMION DM WITH HIGGS PORTAL

In this section, we discuss the simplest Higgs portal singlet fermion DM model with SM gauge invariance and renormalizability. The model contains a SM singlet Dirac fermion DM χ and a singlet scalar mediator S in addition to the SM particles. In order to preserve the SM gauge symmetry, the S only couples to SM particles through the mixing with the SM Higgs h. It is assumed that the DM χ is odd under Z_2 dark parity. Without Z_2 parity, one could write a dim-4 operator, $\bar{l}_L\tilde{H}\chi$, that would make χ decay as forbidden. And this Z_2 distinguishes the DM χ from the right-handed neutrino for neutrino masses and mixings.

The Z_2-invariant Lagrangian related to the DM sector can be written as follows [19]:

$$\begin{aligned}\mathcal{L}_{\rm new} = &\bar{\chi}(i\partial\!\!\!/ - m_\chi - g_\chi S)\chi + \frac{1}{2}\partial_\mu S\partial^\mu S - \frac{1}{2}m_0^2 S^2 \\ &- \lambda_{HS}H^\dagger H S^2 - \mu_0^3 S - \mu_1 S H^\dagger H - \frac{\mu_2}{3!}S^3 - \frac{\lambda_S}{4!}S^4 \ , \end{aligned} \tag{2.1}$$

where H is the SM Higgs doublet. When both scalar fields develop nonzero vacuum expectation value, v_H and v_S, we can expand H and S as

$$H = \begin{pmatrix} G^+ \\ \frac{1}{\sqrt{2}}(v_H + h + iG^0) \end{pmatrix}, \qquad S = v_S + s \ , \tag{2.2}$$

where G^+ and G^0 are Goldstone bosons. Substituting into the Eq. (2.1), we can obtain the mass matrix for physical scalar fields s and h. This mass matrix can be diagonalized by introducing a mixing angle α, which is determined by the λ and μ couplings in the $\mathcal{L}_{\rm new}$. So two mass eigenstates $H_{1,2}$ can be expressed in terms of h and s:

$$\begin{pmatrix} h \\ s \end{pmatrix} = \begin{pmatrix} \cos\alpha & \sin\alpha \\ -\sin\alpha & \cos\alpha \end{pmatrix} \begin{pmatrix} H_1 \\ H2 \end{pmatrix} \ . \tag{2.3}$$

We will take the H_1 as the SM-like Higgs that is consistent with the LHC discovery [28, 29]. So far the measurements of the 125 GeV Higgs boson signal strengths [30, 31] indicate that the mixing angle α is small $\sin\alpha \lesssim 0.4$ [32–34].

The Lagrangian describing the interactions of $H_{1,2}$ with the SM particles and the singlet fermion DM is given by

$$\begin{aligned}\mathcal{L}_{\rm int} = &-(H_1\cos\alpha + H_2\sin\alpha)\left[\sum_f \frac{m_f}{v_h}\bar{f}f - \frac{2m_W^2}{v_h}W_\mu^+ W^{-\mu} - \frac{m_Z^2}{v_h}Z_\mu Z^\mu\right] \\ &+ g_\chi(H_1\sin\alpha - H_2\cos\alpha)\ \bar{\chi}\chi\ . \end{aligned} \tag{2.4}$$

in the mass eigenstates for the neutral scalar bosons.

There are four free parameters relevant to our phenomenological study, m_χ, m_{H_2}, g_χ and $\sin\alpha$. Moreover, there could be new decay modes open for the H_2, such as $H_2 \to H_1 H_1$ if kinematically allowed. And we will see later that the total decay width of H_2 (Γ_{H_2}) is playing a very important role in reconstructing observables at detector level through interference between H_1 and H_2 propagators. Therefore Γ_{H_2} will be treated as the fifth free parameter in the following discussion.

III. THE INTERFERENCE EFFECT BETWEEN TWO SCALAR MEDIATORS AT LHC

In the singlet fermion DM model with Higgs portal described in the previous section, the DM production is dominated by three processes as shown in Fig. 1: i.e. gluon-gluon fusion (ggF), vector boson fusion (VBF) and Higgs Strahlung (VH).

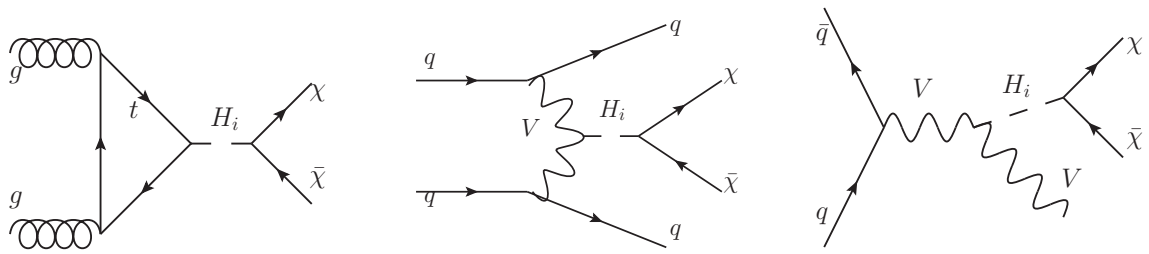

FIG. 1: The dominant DM production processes at LHC.

In contrast to the simplified scalar mediated DM model recommended by the LHC Dark Matter Forum [11], there are two propagators (H_1 and H_2) that can mediate the DM pair production in the gauge invariant model descried in the previous section. Note that the Lagrangian in Eq. (2.4) resembles the singlet scalar mediated DM model in Ref. [11] when only fermionic couplings of H_2 are concerned.

The interference between two propagators in the differential production cross sections of the DM pair take the following form:

$$\frac{d\sigma_i}{dm_{\chi\chi}} \propto \left|\frac{\sin 2\alpha\ g_\chi}{m_{\chi\chi}^2 - m_{H_1}^2 + i m_{H_1}\Gamma_{H_1}} - \frac{\sin 2\alpha\ g_\chi}{m_{\chi\chi}^2 - m_{H_2}^2 + i m_{H_2}\Gamma_{H_2}}\right|^2 , \tag{3.1}$$

where σ_i corresponds to the cross section of given production process and $m_{\chi\chi}$ is the invariant mass of DM pair. The minus sign between two propagators comes from the $SO(2)$ nature of the mixing matrix in Eq. (2.3), which is found to be helpful to evade the DM direct detection [19, 35] in such class of models. The interference effect will not only influence the total production rate of DM pair, but also change the shape of kinematic variables.

To give more concrete examples on the interference effect, a few assumptions are made to narrow down the parameter space. We will fix $\sin\alpha = 0.2$ and $g_\chi = 1$ in our following discussion. Because the differential cross section are universally proportional to $g_\chi \sin 2\alpha$ as shown in Eq. (3.1), changing the $\sin\alpha$ and g_χ will simply rescale the differential cross section as long as the Γ_{H_i} does not differ much. The scalar H_1 is identified as the 125 GeV Higgs boson with properties that are consistent with the LHC discovery, so that $m_{H_1} = 125$ GeV and $\Gamma_{H_1} = \cos^2\alpha \cdot \Gamma_{h_{\rm SM}}$. Models with $m_\chi < m_{h_{\rm SM}}/2$ will be highly constrained by the Higgs invisible decay search at LHC. This usually requires very small g_χ, e.g. for $\sin\alpha = 0.2$, g_χ should be smaller than $\lesssim 0.1$ in order to satisfy the current upper bound on the invisible Higgs branching ratio: $\mathrm{Br}(h_{\rm SM} \to \chi\chi) < 0.24$ [36]. Then the DM production cross section should be small in such cases. The same situation exists when DM is heavy. So we will focus on the scenarios with medium DM mass in this work, which we choose $m_\chi = 80$ GeV without lose of generality. Then we are left with two most relevant parameters: m_{H_2} and Γ_{H_2}.

The FeynRules [37]/MadGraph5_aMC@NLO [38] framework is used in order to calculate the NLO QCD cross sections and simulate the events. The FeynRules takes the Lagrangian of the simplified model in Eq. (2.4) as well as the UV/R_2 counterterms for the NLO QCD computations from NLOCT [39]/FeynArts [40] to generate the Universal FeynRules Output model files. The MadGraph5_aMC@NLO uses the model files to compute the tree-level and loop-level amplitudes for any processes of the model.

We calculate the Leading-Order (LO) cross section of the gluon-gluon fusion DM pair production by using the loop induced mode [41] of MadGraph5_aMC@NLO. The results for varying m_{H_2} and Γ_{H_2} are shown in Fig. 2.

In the figure, the $\Gamma_{\rm min}$ for H_2 is calculated by assuming H_2 decays only into SM particles and DM pair through the interactions given in Eq. (2.4), where we have set $\sin\alpha = 0.2$ and $g_\chi = 1$. Note that the actual H_2 decay width could be larger than $\Gamma_{\rm min}$, if $H_2 \to H_1 H_1$ is open and non-negligible, or if there are other decay channels of H_2. For example, there could be extra dark sector particles such as dark Higgs or dark gauge bosons if Z_2 symmetry is replaced by dark gauge symmetry (see Refs. [42, 43] for example). These extra channels are more model dependent though. Therefore we consider three different widths of H_2 throughout the work: $\Gamma_{\rm min}$, $5 \times \Gamma_{\rm min}$ and $20 \times \Gamma_{\rm min}$, respectively. The lines associate to $H_1\&H_2$ and H_2 are calculated with and without the H_1 as the mediator respectively. The former case corresponds to the gauge invariant singlet fermion DM models with Higgs portal, while the later case corresponds to the usual singlet scalar portal DM model as proposed in Ref. [11] and widely used in literature.

From Fig. 2, we can observe that including the H_1 will substantially reduce the DM pair production cross section when $m_{H_2} \lesssim 2m_\chi$. This is because of the destructive interference between two mediators caused by the minus sign in Eq. (3.1). Note that the collider signatures in this parameter region have not been studied carefully in previous studies of the singlet fermion DM model with Higgs portal except in Ref. [17], partly because the signal cross section is expected to be small. Our study in the present work shows that the signal cross section is even smaller than that of the simplified model with a single scalar mediator

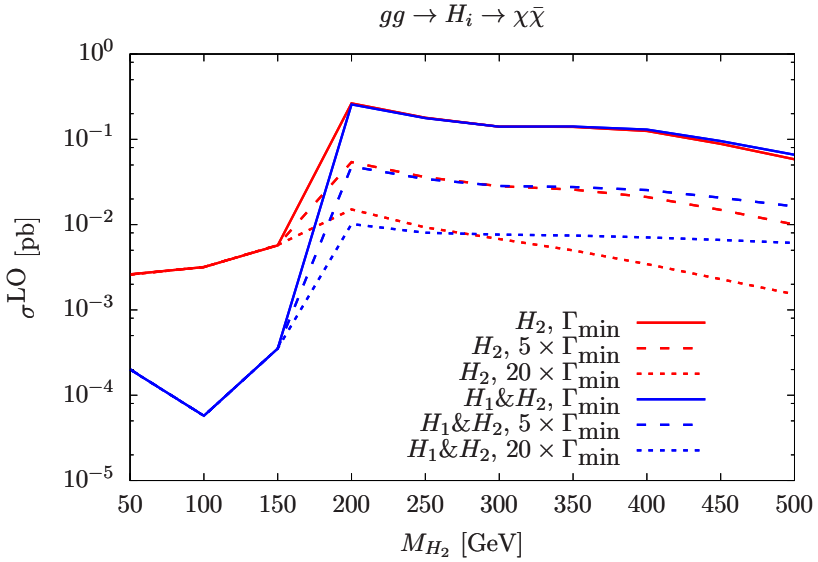

FIG. 2: The LO cross section for gluon-gluon fusion process at 13 TeV LHC. The meanings of the different line types are explained in the text and the similar strategy will be used in all figures.

which is violating the full SM gauge invariance.

Once the $m_{H_2} \gtrsim 2m_\chi$, the cross section increases dramatically due to resonant enhancement [1]. From Eq. 3.1, we know the contributions of two propagators interfering constructively in the region $m_{\chi\chi} \in [2m_\chi, m_{H_2})$ and destructively in the region $m_{\chi\chi} \in (m_{H_2}, +\infty)$. When m_{H_2} is not much larger than twice of DM mass, the destructive effect dominates. As the H_2 becomes heavier ($\gtrsim 270$ GeV in our parameter setup), there are more fraction of events falling into the constructive region. This explains why the $H_1\&H_2$ scenario has smaller cross section than the usual H_2 scenario when $m_{H_2} \in (2m_{\chi\chi}, \sim 270$ GeV) and larger cross section when $m_{H_2} \gtrsim 270$ GeV. Such features will become even more significant for wider decay width of H_2 as we can expect. Given $m_{H_2} = 400$ GeV as an example, the difference in total cross section is $\frac{\sigma(H_1\&H_2)-\sigma(H_2)}{\sigma(H_2)} \sim 4\%$ for $\Gamma_{H_2} = \Gamma_{\rm min}$ while can be as large as $\sim 106\%$ for $\Gamma_{H_2} = 20 \times \Gamma_{\rm min}$.

To see the interference effect more explicitly, we plot the differential cross section in $m_{\chi\chi}$ for the ggF process in Fig. 3. Two different masses of H_2 are considered with the DM mass being fixed to 80 GeV. For both masses, we can observe the enhancement in event fraction for $m_{\chi\chi} \in (2m_\chi, m_{H_2})$ and deduction in event fraction when $m_{\chi\chi} > m_{H_2}$. For $m_{H_2} = 200$ GeV, the total event fraction in $(2m_\chi, m_{H_2})$ is smaller than that in $(m_{H_2}, +\infty)$ while it is opposite for $m_{H_2} = 400$ GeV. Note that for heavy mass and large decay width of H_2, the resonant peak can be smeared out as shown by the solid blue curve in the right panel due to the significant enhancement from the interference effect between H_1 and H_2.

So far, we have discussed the features of the interference effect at parton level for $gg \to H_i \to \chi\chi$. In practice, there will be extra radiations from the gluons in initial state and top quarks in the loop, which may affect the features of interference to some extent. Moreover, the variable $m_{\chi\bar{\chi}}$ is not a physical observable at hadron colliders since it cannot

[1] In this mass region, the $H_1\&H_2$ scenario can be effectively described by the H_2 scenario only when the decay width of H_2 is narrow and the mass of H_2 is relatively light.

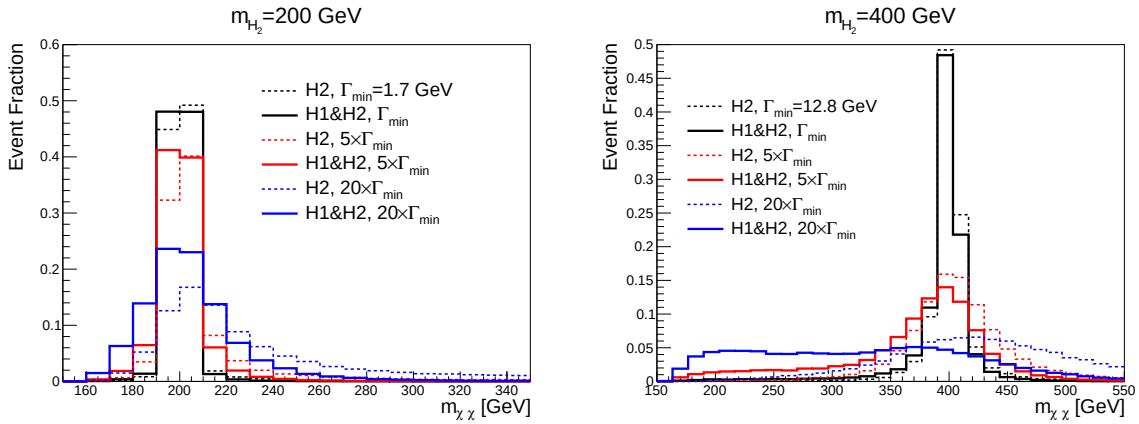

FIG. 3: The parton level distributions of $m_{\chi\bar{\chi}}$ for gluon-gluon fusion process at 13 TeV LHC.

be reconstructed there. In order to obtain a more realistic results on the interference effect to a realistic DM search at hadron collider, we need to include those radiations in our events simulation and present the result with a more realistic and measurable observable.

In a typical DM search at the LHC, one usually requires an energetic jet in the final state, i.e. mono-jet search. So we generate the DM pair production in associate with an extra jet at parton level. The events are passed to Pythia6 [44] for parton showering and hadronization. The final state particles are used for reconstructing the physical objects such as isolated lepton and jets. Jets are clustered using the anti-k_t algorithm [45] with distance parameter of $R = 0.4$ as implemented in Fastjet [46]. The benchmark points with $m_{H_2} = 400$ GeV and three different decay widths for H_2 are chosen for representative study because the interference effect here is relatively large.

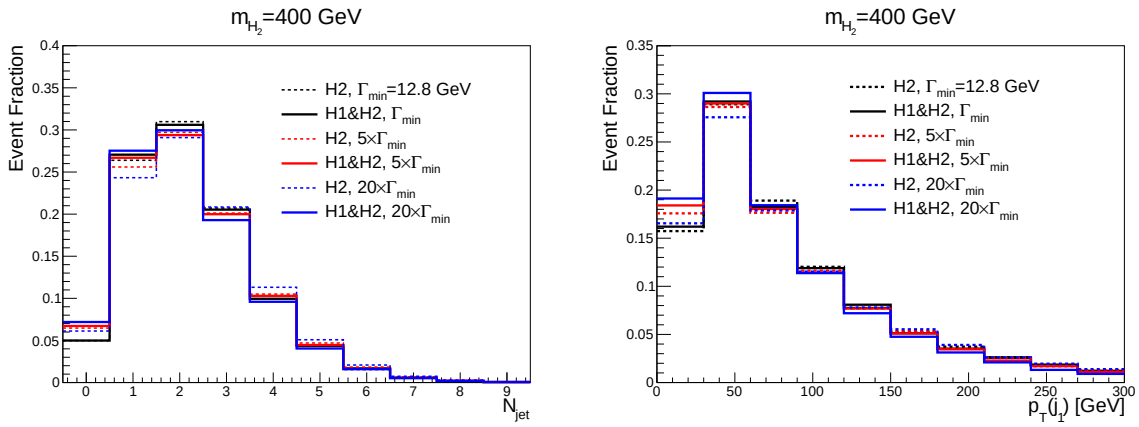

FIG. 4: The distributions of the number of reconstructed jets (left) and the transverse momentum of the leading jet (right) for ggF process at 13 TeV LHC, including the radiation of an extra jet and parton shower effect.

The distributions of reconstructed jet number $N_{\rm jet}$ and leading jet transverse momentum $p_T(j_1)$ are shown in Fig. 4. The jets are required to have $p_T(j) > 20$ GeV and $|\eta(j)| < 4.5$. Both the frequency and the energy of jet radiation are proportional to the energy scale of a event, which is given by $m_{\chi\chi}$. And the interference effect tends to increase the event rate in

low $m_{\chi\chi}$ region and reduce the event rate in high $m_{\chi\chi}$ region. As a result, we can observe that the $H_1\&H_2$ scenario has lower jet multiplicity and softer $p_T(j_1)$ distribution comparing to the H_2 scenarios. The differences become larger for wider H_2 decay width.

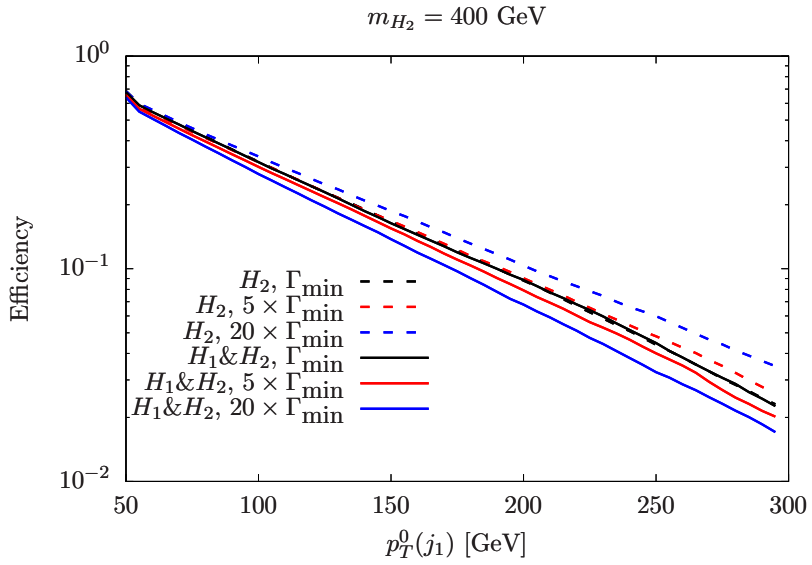

FIG. 5: The cumulative curve of the $p_T(j_1)$ distribution in ggF process at 13 TeV LHC.

A DM search at the LHC usually counts the number of events that pass certain cuts, e.g. $p_T(j_1) > 200$ GeV. Thus the efficiency of the cut is directly related to the search sensitivity. The efficiency for a given cut $p_T(j_1) > p_T^0(j_1)$ is calculated by integrating the $p_T(j_1)$ distribution in the right panel of Fig. 4 from $p_T^0(j_1)$ to infinity, i.e. the cumulative curve. We present the cumulative curves for different scenarios in Fig. 5. The difference in efficiencies between $H_1\&H_2$ and H_2 scenarios becomes more significant for more stringent $p_T(j_1)$ cut and/or larger H_2 decay width. For example, when H_2 width is large $20\times\Gamma_{\rm min}$, the efficiency ratios (defined as $\frac{\epsilon(H_1\&H_2)}{\epsilon(H_2)}$) are 0.83 and 0.66 for $p_T(j_1) > 100$ GeV and $p_T(j_1) > 200$ GeV cuts, respectively. As for narrower H_2 width $5\times\Gamma_{\rm min}$ the corresponding efficiency ratios are 0.95 and 0.88.

IV. THE LHC SEARCH BOUNDS

Motivated by the gauge invariance of simplified Higgs portal DM models, we have found that the existence of the additional SM-like Higgs H_1 propagator could affect the LHC DM search, both on total production rate and shape of kinematic variables. In this section, we will demonstrate the importance of this influence in a practical analysis at the LHC.

In Ref. [47], the CMS collaboration reported DM searches in final states with either an energetic jet or a boosted hadronically decaying vector boson using 12.9 fb^{-1} data set at 13 TeV. The search is especially relevant to our simplified model in which two Higgs bosons couple strongly to top quark and vector boson. In their search, two classes of cuts are designed aiming for the energetic jet and boosted boson respectively.

- Mono-jet cuts: (1). Events are required to have missing transverse momentum $p_T^{\rm miss} > 200$ GeV. (2). A event is vetoed if it contains any isolated leptons, isolated photons,

τ-tagged jets and b-tagged jets. (3). The jets are clustered using anti-k_t algorithm with $R = 0.4$ (denoted by $j^{\rm ak4}$). The leading $j^{\rm ak4}$ is required to have $p_T(j_1^{\rm ak4}) > 100$ GeV and $|\eta(j_1^{\rm ak4})| < 2.5$. (4). The minimum azimuthal angle between the $\vec{p}_T^{\rm miss}$ and leading four $j^{\rm ak4}$s with $p_T > 30$ GeV is required to be greater than 0.5.

- Mono-V cuts: (1). A more stringent cut on $p_T^{\rm miss}$ is applied, $p_T^{\rm miss} > 250$ GeV. (2). The final states particles are reclustered using anti-k_t algorithm with $R = 0.8$, denoted by $j^{\rm ak8}$. The leading $j^{\rm ak8}$ should has $p_T(j_1^{\rm ak4}) > 250$ GeV and $|\eta(j_1^{\rm ak8})| < 2.4$. (3). Invariant mass of the leading $j^{\rm ak8}$ after pruning [48] is required to be between 65 and 105 GeV. (4). The N-subjettiness variable τ_N [49] is used to discriminate the two prong decays of the vector boson from QCD jets. The leading $j^{\rm ak8}$ is required to have $\tau_2/\tau_1 < 0.6$.

Two signal regions (SR) are defined in their analysis based on above cuts: the mono-jet SR and mono-V SR. Events that pass both mono-jet cuts and mono-V cuts are assigned to the mono-V SR. And those that pass the mono-jet cuts while fails any of these mono-V cuts are assigned to the mono-jet SR. By recasting their analysis on the SM Higgs invisible decay and comparing with their results given in the Fig.15 of Ref. [47], we can find that the 95% CL expected upper limit on the number of new physics events in mono-jet SR ($N^{\rm upper}_{\text{mono-jet}}$) and mono-V SR ($N^{\rm upper}_{\text{mono-V}}$) are around 10833 and 447.2, respectively. The upper bound will be projected to our simplified Higgs portal DM model with either one or two scalar bosons.

The DM pair can be produced by three processes in our model as shown in Fig. 1. The ggF process itself does not produce any observable signals at detector. Extra energetic jets radiation from either initial state gluon or top quark in the loop can circumvent this issue. The LO cross section for DM pair production in association with a jet is computed by the MadGraph5_aMC@NLO, where the jet is required to have $p_T(j) > 100$ GeV. Meanwhile, the higher order corrections are found to be quite significant in improving the ggF cross section in Higgs production. Using the SusHi program [50–52], the NNLO K-factors for Higgs mass $\in [100, 500]$ are calculated to be around 2.5. So the production cross section for the ggF process is given by multiplying the LO cross section in MadGraph5_aMC@NLO with a universal K-factor of 2.5. Two forward/backward jets are produced in associate with DM pair in VBF processes. The correction to the inclusive VBF Higgs production cross section up to NNLO is found to be only around percent level [53]. So the LO cross section for DM production in VBF process can be used directly, where we only impose mild cuts on forward/backward jets, $p_T(j) > 20$ GeV and $|\eta(j)| < 4.5$. As for the VH process, we include all three vector bosons $W^\pm$ and Z in the final state. Even though only hadronically decaying Vs are considered in the CMS analysis, we do not include the decay branching ratio of the vector bosons when calculating the DM production cross section. The NLO cross section in QCD is calculated by the MadGraph5_aMC@NLO.

In Fig 6, we plot the cross sections of three DM production processes at the 13 TeV LHC. The main features of this figure regarding the variations of m_{H_2} and $\Gamma(H_2)$ follow the general arguments that are conducted for Fig. 2. Beside those, we can observe that the ggF is the most dominant production process even after applying the stringent cut on the radiated jet. The cross section of VH is around one to two orders of magnitude smaller than that of ggF. Among three DM production processes, the interference effect between two propagators is most significant in VH process. This is because the VH process has higher energy scale than ggF/VBF process due to the heavy vector boson in the final state. The fact that the parton distribution function of proton favoring small x (which is the energy fraction for a given

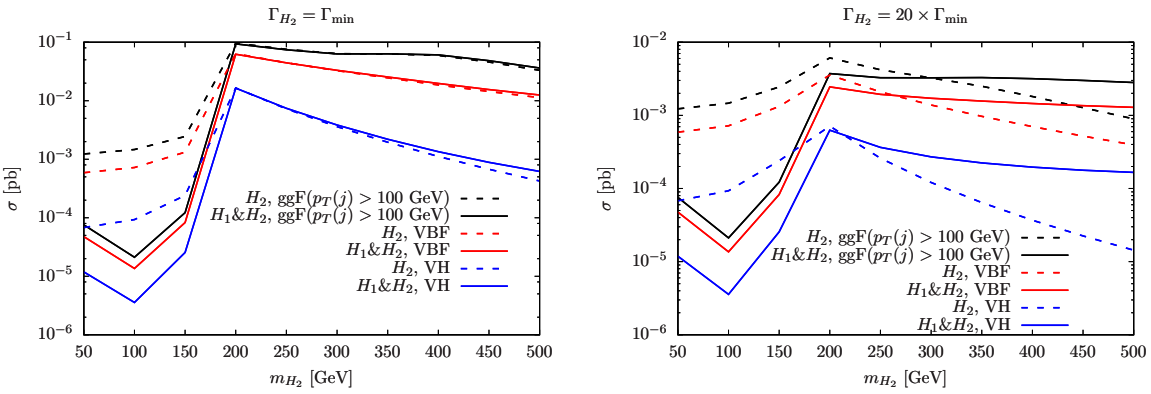

FIG. 6: The production cross sections for ggF (black), VBF (red) and VH (blue) processes at 13 TeV LHC. Left panel: The decay width of H_2 is $\Gamma_{\rm min}$. Right panel: A relatively large decay width of H_2 is chosen, $20 \times \Gamma_{\rm min}$. The difference between the solid and the dashed lines with the same color show the importance of the interference effects from two scalar boson propagators.

parton inside the proton) helps to increase the production probability in the low energy scale region, i.e. the constructive interference region.

Next, we should simulate events for calculation of the signal efficiencies in mono-jet search and mono-V search. Signal events are simulated based on the FeynRules/MadGraph5_aMC@NLO framework as introduced before. The Pythia6 is used for decaying the vector boson in VH process, as well as for parton showering and hadronization. The realistic detector effects are simulated by the Delphes3 [54]. For each production process, the same cuts that used in computing the cross section are used in event generation.

Three production processes are analyzed individually. The signal efficiency of mono-jet/mono-V search for a given benchmark point in a production process is defined as the ratio between the number of signal events in mono-jet/mono-V SR and the total number of simulated events. In order to show the influence of the interference effect to signal efficiency, we plot the efficiency ratios between signals with and without H_1, i.e. $\epsilon(H_1\&H_2)/\epsilon(H_2)$, for different production processes with varying Γ_{H_2} and m_{H_2} in Fig. 7.

As we can see from the figure, because the interference effect always enhances the production rate in low energy scale region, the efficiency ratios are smaller than one in most cases. In mono-jet search, when $m_{H_2} < 2m_\chi$, the amplitudes of the Feynman diagrams with H_1 and H_2 propagators are of similar size, so the destructive interference effect is significant, especially in the high energy scale region. When the H_2 is not so heavy and has small decay width, the amplitude of H_2 becomes dominant once it goes on-shell, $m_{H_2} > 2m_\chi$. Then, the interference effect is negligible. The interference effect is more important for scenarios with wider H_2 decay width. For $m_{H_2} \in [50, 500]$ GeV and $\Gamma(H_2) = 20 \times \Gamma_{\rm min}$ the interference effect can change the signal efficiency by around 20% in ggF and VBF production processes. The VH process is most sensitive to the interference effect because of the higher energy scale, where the efficiency ratio decrease quickly as increasing either m_{H_2} or $\Gamma(H_2)$. For $m_{H_2} = 500$ GeV and $\Gamma(H_2) = 20 \times \Gamma_{\rm min}$, the $\epsilon(H_1\&H_2)/\epsilon(H_2)$ in VH process can be as low as $\sim 50\%$, while it is $\sim 80\%$ for $\Gamma(H_2) = \Gamma_{\rm min}$ or $m_{H_2} = 200$ GeV. Comparing to the mono-jet search, the typical signal efficiency in the mono-V search is more than one order of magnitude smaller, thus larger fluctuations of efficiency ratios due to lower statistics are

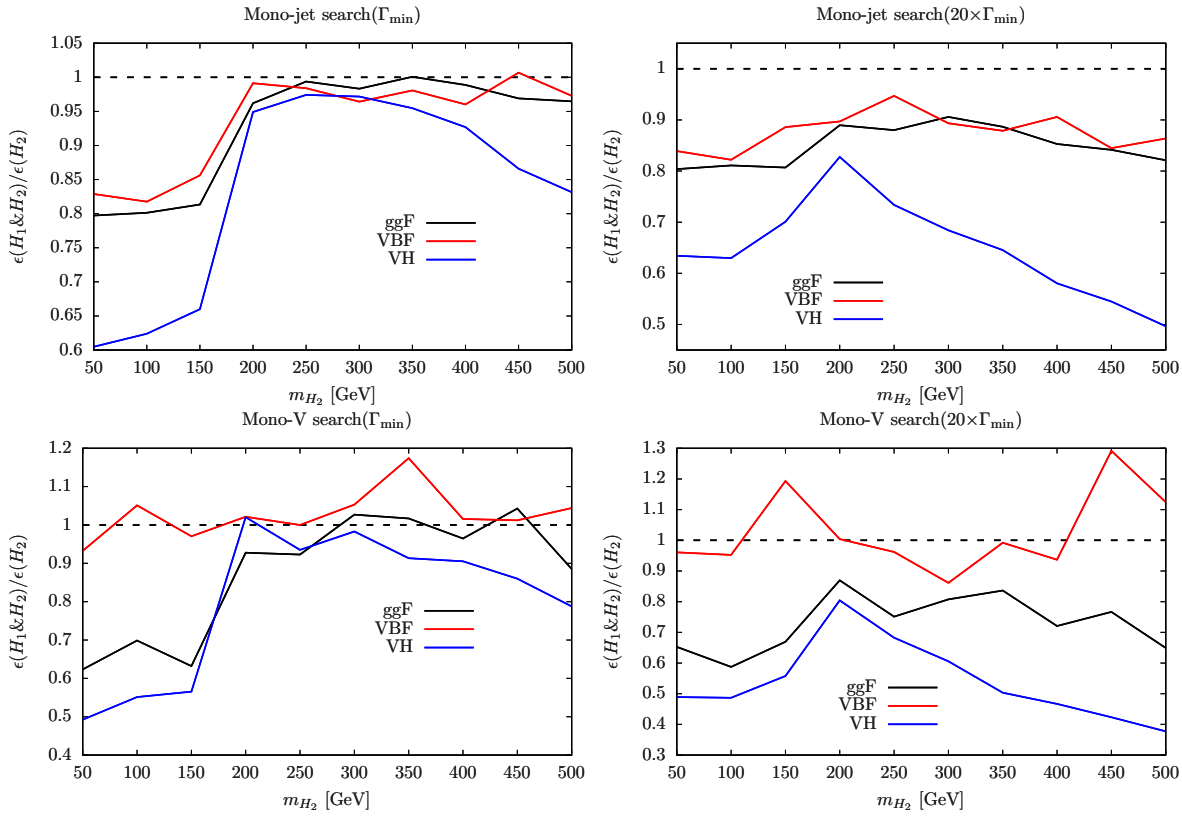

FIG. 7: The cut efficiency ratios for mono-jet search (upper panels) and mono-V search (lower panels) in different production processes. Left panels: The decay width of H_2 is $\Gamma_{\rm min}$. Right panels: A relatively large decay width of H_2 is chosen, $20 \times \Gamma_{\rm min}$.

observed. For ggF and VH processes, the main trends of $\epsilon(H_1\&H_2)/\epsilon(H_2)$ with varying m_{H_2} and $\Gamma(H_2)$ follow that in the mono-jet search, with an overall shifting downward. On the other hand, the efficiency ratio of VBF process is quite insensitive to the interference effects in the mono-V search, irrespective of the H_2 decay width.

Known the production cross sections and the signal efficiencies, we now able to calculate the CMS search constraints on our models. For a given parameter point, the number of signal events in the mono-jet/mono-V SR is calculated by $\mathcal{L} \times \sigma_i \times \epsilon_i^{\text{mono-jet/mono-V}}$, where $\mathcal{L} = 12.9$ fb^{-1} is integrated luminosity and i indicates the production process, ggF, VBF or VH. The contributions from all three production processes are added up which will be compared with the $N^{\text{upper}}_{\text{mono-jet}}$ in mono-jet search and $N^{\text{upper}}_{\text{mono-V}}$ in mono-V search. The limit on the signal strength

$$\mu_{\text{mono-jet/mono-V}} = \frac{\sigma}{\sigma_{\text{theory}}} = \frac{N^{\text{upper}}_{\text{mono-jet/mono-V}}}{\sum_{i=\text{ggF, VBF, VH}} \mathcal{L} \times \sigma_i \times \epsilon_i^{\text{mono-jet/mono-V}}} \tag{4.1}$$

for $H_1\&H_2$ and H_2 scenarios are plotted in Fig. 8.

From Fig. 8 we can observe that the features of the exclusion bounds are approximately described by the inverse of the production cross sections. In the light H_2 region $m_{H_2} < 2m_\chi$, the reduction of cross section due to destructive interference leads to very weak bound in the $H_1\&H_2$ scenario. The bounds become much more stringent when $m_{H_2} \gtrsim 2m_\chi$ because of the resonant enhancement, especially for narrow decay width of H_2. However, the interference

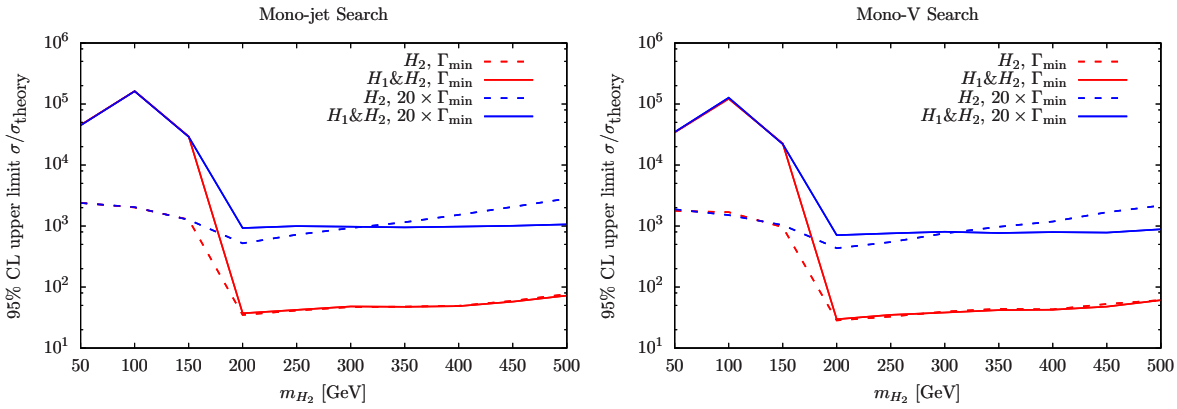

FIG. 8: The CMS exclusion limits on our simplified models. Left: upper limit from mono-jet search. Right: upper limit from mono-V search.

effect on signal efficiencies also play non-negligible roles in the exclusion bounds. As we have discussed for Fig. 2, the interference effect on cross section leads to smaller cross section when $m_{H_2} \in (2m_{\chi\chi}, 270\ \text{GeV})$ and larger cross section when $m_{H_2} > 270$ GeV. The reduction of signal efficiency from interference effect will the enlarge the difference in search sensitivities for $m_{H_2} \in (2m_{\chi\chi}, 270\ \text{GeV})$ and shrink it for $m_{H_2} > 270$ GeV, as can be seen clearly from the solid and dashed blue curves in Fig. 8. Among two searches, the mono-V search has slightly better sensitivity than the mono-jet search. Both of them are indicating that the signal cross section in our model is at least one order of magnitude below the current reach. This is mainly because of the suppression factor of $\sin^2 2\alpha$ in all DM production cross sections. Much larger data set or/and higher hadron collision energy are expected to probe our models.

	Mono-jet SR			Mono-V SR		
	ggF	VBF	VH	ggF	VBF	VH
$H_2, \Gamma_{\rm min}$	194.4	22.3	2.9	7.8	1.2	1.4
$H_1\&H_2, \Gamma_{\rm min}$	197.0	22.7	3.2	7.7	1.3	1.5
$H_2, 20\times\Gamma_{\rm min}$	6.2	0.82	0.092	0.28	0.049	0.043
$H_1\&H_2, 20\times\Gamma_{\rm min}$	9.2	1.5	0.28	0.36	0.094	0.11

TABLE I: The number of events of different production processes in mono-jet SR and mono-V SR for each signal process with $m_{H_2} = 400$ GeV at 12.9 fb^{-1} 13 TeV LHC.

The composition of the DM signal in the mono-jet SR and the mono-V SR in terms of three production processes for the benchmark point with $m_{H_2} = 400$ GeV are provided in Table I. For mono-jet search, the ggF is always the most dominant process, the composition of which is around one order of magnitude larger than that of VBF and around two orders of magnitude larger than that of VH process. The VH becomes much more important in the mono-V search, whose composition is only a few times smaller than that of ggF. Note that in mono-V search, there are still large contributions from ggF due the mis-tagging of boosted vector boson jet. We would also like to point out that the interference effect tends to increase the composition of VH in both SRs, especially for the scenario with large H_2 decay width.

V. CONCLUSIONS

In this paper, we have considered the collider phenomenology of a gauge invariant and renormalizable model for singlet fermion DM with Higgs portal. In this model, there appear two neutral scalar bosons formed by the mixing of the singlet and the doublet Higgs bosons that could mediate the DM production. In certain kinematic regions, their interference can affect the signal in either destructive or constructive manners. This leads to very important applications to the DM searches at the LHC which have been largely ignored in the previous study except in Ref. [16, 17].

Due to the minus sign in the scalar mixing matrix (2.3), the DM production rate is enhanced in the kinematic region where $m_{H_1} < m_{\chi\chi} < m_{H_2}$ and suppressed in the region of $m_{\chi\chi} < m_{H_1}$ or $m_{\chi\chi} > m_{H_2}$, thus affecting both DM production cross sections and final state distributions. The cross section will be reduced substantially when the $m_{H_2} < 2m_\chi$, thereby rendering the collider search for DM less effective than naively expected from the simplified model without the SM Higgs-like H_1 propagator. For $m_{H_2} > 2m_\chi$, the interference effect in cross section changes from destructive to constructive one with increasing the H_2 mass. Assuming $m_{H_1} < 2m_\chi$, such that the SM Higgs invisible decay is kinematically forbidden, the interference effect always enhances the signal events in the low $m_{\chi\chi}$ region. Since the frequency and the energy of the jet radiation are proportional to $m_{\chi\chi}$, lower jet multiplicity and less energetic jets in the final state are obtained. We also find the interference effect becomes more important for larger decay width of H_2.

The CMS search for DM in final states with either an energetic jet or a boosted hadronically decaying vector boson has been applied to scenarios with and without H_1. The interference effect will dramatically reduce the sensitivity in the parameter region $m_{H_2} < 2m_\chi$ while the suppression is only mild when m_{H_2} becomes slightly higher than $2m_\chi$. The sensitivity can even be enhanced when H_2 is significantly higher than $2m_\chi$. In our model setup the production cross section of DM signals is more than one order of magnitude below the current LHC search sensitivity, mainly because of the small factor $\sin^2 2\alpha$ in production cross section.

ACKNOWLEDGMENTS

This work is supported in part by National Research Foundation of Korea (NRF) Research Grant NRF-2015R1A2A1A05001869 (PK, JL), and by the NRF grant funded by the Korea government (MSIP) (No. 2009-0083526) through Korea Neutrino Research Center at Seoul National University (PK).

[1] Planck collaboration, P. A. R. Ade et al., Planck 2015 results. XIII. Cosmological parameters, Astron. Astrophys. **594** (2016) A13, [1502.01589].

[2] J. Goodman, M. Ibe, A. Rajaraman, W. Shepherd, T. M. P. Tait and H.-B. Yu, Constraints on Light Majorana dark Matter from Colliders, Phys. Lett. **B695** (2011) 185–188, [1005.1286].

[3] J. Goodman, M. Ibe, A. Rajaraman, W. Shepherd, T. M. P. Tait and H.-B. Yu, Constraints on Dark Matter from Colliders, Phys. Rev. **D82** (2010) 116010, [1008.1783].

[4] M. Duch, B. Grzadkowski and J. Wudka, Classification of effective operators for interactions between the Standard Model and dark matter, JHEP **05** (2015) 116, [1412.0520].

[5] O. Buchmueller, M. J. Dolan and C. McCabe, Beyond Effective Field Theory for Dark Matter Searches at the LHC, JHEP **01** (2014) 025, [1308.6799].

[6] G. Busoni, A. De Simone, E. Morgante and A. Riotto, On the Validity of the Effective Field Theory for Dark Matter Searches at the LHC, Phys. Lett. **B728** (2014) 412–421, [1307.2253].

[7] G. Busoni, A. De Simone, J. Gramling, E. Morgante and A. Riotto, On the Validity of the Effective Field Theory for Dark Matter Searches at the LHC, Part II: Complete Analysis for the s-channel, JCAP **1406** (2014) 060, [1402.1275].

[8] G. Busoni, A. De Simone, T. Jacques, E. Morgante and A. Riotto, On the Validity of the Effective Field Theory for Dark Matter Searches at the LHC Part III: Analysis for the t-channel, JCAP **1409** (2014) 022, [1405.3101].

[9] J. Abdallah et al., Simplified Models for Dark Matter and Missing Energy Searches at the LHC, 1409.2893.

[10] J. Abdallah et al., Simplified Models for Dark Matter Searches at the LHC, Phys. Dark Univ. **9-10** (2015) 8–23, [1506.03116].

[11] D. Abercrombie et al., Dark Matter Benchmark Models for Early LHC Run-2 Searches: Report of the ATLAS/CMS Dark Matter Forum, 1507.00966.

[12] M. R. Buckley, D. Feld and D. Goncalves, Scalar Simplified Models for Dark Matter, Phys. Rev. **D91** (2015) 015017, [1410.6497].

[13] P. Harris, V. V. Khoze, M. Spannowsky and C. Williams, Constraining Dark Sectors at Colliders: Beyond the Effective Theory Approach, Phys. Rev. **D91** (2015) 055009, [1411.0535].

[14] P. Harris, V. V. Khoze, M. Spannowsky and C. Williams, Closing up on Dark Sectors at Colliders: from 14 to 100 TeV, Phys. Rev. **D93** (2016) 054030, [1509.02904].

[15] V. V. Khoze, G. Ro and M. Spannowsky, Spectroscopy of scalar mediators to dark matter at the LHC and at 100 TeV, Phys. Rev. **D92** (2015) 075006, [1505.03019].

[16] P. Ko. 2015. Invited talks by at Mitchell Workshop on Collider and Dark Matter Physics, May 12-15 , Texas A&M, USA. https://indico.cern.ch/event/283774 2015. The 16th LHC monthly workshop, June 1-2 , KIAS, Seoul, Korea. http://home.kias.re.kr/MKG/h/LHC16/ 2015. CosKASI Dark Matter Workshop, June 9-11 , KASI, Daejon, Korea. http://cosmology.kasi.re.kr/dmworkshop2015/home.html

[17] S. Baek, P. Ko, M. Park, W.-I. Park and C. Yu, Beyond the Dark matter effective field theory and a simplified model approach at colliders, Phys. Lett. **B756** (2016) 289–294, [1506.06556].

[18] C. Englert, M. McCullough and M. Spannowsky, S-Channel Dark Matter Simplified Models and Unitarity, 1604.07975.

[19] S. Baek, P. Ko and W.-I. Park, Search for the Higgs portal to a singlet fermionic dark matter at the LHC, JHEP **02** (2012) 047, [1112.1847].

[20] S. Baek, P. Ko, W.-I. Park and E. Senaha, Higgs Portal Vector Dark Matter : Revisited, JHEP **05** (2013) 036, [1212.2131].
[21] M. Bauer et al., Towards the next generation of simplified Dark Matter models, 1607.06680.
[22] P. Ko and H. Yokoya, JHEP **1608**, 109 (2016) doi:10.1007/JHEP08(2016)109 [arXiv:1603.04737 [hep-ph]].
[23] N. F. Bell, Y. Cai and R. K. Leane, arXiv:1610.03063 [hep-ph].
[24] N. F. Bell, Y. Cai, J. B. Dent, R. K. Leane and T. J. Weiler, Dark matter at the LHC: Effective field theories and gauge invariance, Phys. Rev. **D92** (2015) 053008, [1503.07874].
[25] A. Choudhury, K. Kowalska, L. Roszkowski, E. M. Sessolo and A. J. Williams, Less-simplified models of dark matter for direct detection and the LHC, JHEP **04** (2016) 182, [1509.05771].
[26] F. Kahlhoefer, K. Schmidt-Hoberg, T. Schwetz and S. Vogl, Implications of unitarity and gauge invariance for simplified dark matter models, JHEP **02** (2016) 016, [1510.02110].
[27] P. Ko, A. Natale, M. Park and H. Yokoya, Simplified DM models with the full SM gauge symmetry : the case of t-channel colored scalar mediators, 1605.07058.
[28] ATLAS collaboration, G. Aad et al., Observation of a new particle in the search for the Standard Model Higgs boson with the ATLAS detector at the LHC, Phys. Lett. **B716** (2012) 1–29, [1207.7214].
[29] CMS collaboration, S. Chatrchyan et al., Observation of a new boson at a mass of 125 GeV with the CMS experiment at the LHC, Phys. Lett. **B716** (2012) 30–61, [1207.7235].
[30] CMS collaboration, V. Khachatryan et al., Precise determination of the mass of the Higgs boson and tests of compatibility of its couplings with the standard model predictions using proton collisions at 7 and 8 TeV, Eur. Phys. J. **C75** (2015) 212, [1412.8662].
[31] ATLAS collaboration, G. Aad et al., Measurements of the Higgs boson production and decay rates and coupling strengths using pp collision data at $\sqrt{s} = 7$ and 8 TeV in the ATLAS experiment, Eur. Phys. J. **C76** (2016) 6, [1507.04548].
[32] T. Robens and T. Stefaniak, Eur. Phys. J. C **75**, 104 (2015) doi:10.1140/epjc/s10052-015-3323-y [arXiv:1501.02234 [hep-ph]].
[33] K. Cheung, P. Ko, J. S. Lee and P. Y. Tseng, JHEP **1510**, 057 (2015) doi:10.1007/JHEP10(2015)057 [arXiv:1507.06158 [hep-ph]].
[34] G. Dupuis, JHEP **1607**, 008 (2016) doi:10.1007/JHEP07(2016)008 [arXiv:1604.04552 [hep-ph]].
[35] M. Duerr, F. Kahlhoefer, K. Schmidt-Hoberg, T. Schwetz and S. Vogl, How to save the WIMP: global analysis of a dark matter model with two s-channel mediators, JHEP **09** (2016) 042, [1606.07609].
[36] CMS collaboration, Searches for invisible Higgs boson decays with the CMS detector., CMS-PAS-HIG-16-016 (2016) .
[37] A. Alloul, N. D. Christensen, C. Degrande, C. Duhr and B. Fuks, FeynRules 2.0 - A complete toolbox for tree-level phenomenology, Comput. Phys. Commun. **185** (2014) 2250–2300, [1310.1921].
[38] J. Alwall, R. Frederix, S. Frixione, V. Hirschi, F. Maltoni, O. Mattelaer et al., The automated computation of tree-level and next-to-leading order differential cross sections, and

their matching to parton shower simulations, JHEP **07** (2014) 079, [1405.0301].
[39] C. Degrande, Automatic evaluation of UV and R2 terms for beyond the Standard Model Lagrangians: a proof-of-principle, Comput. Phys. Commun. **197** (2015) 239–262, [1406.3030].
[40] T. Hahn, Generating Feynman diagrams and amplitudes with FeynArts 3, Comput. Phys. Commun. **140** (2001) 418–431, [hep-ph/0012260].
[41] V. Hirschi and O. Mattelaer, Automated event generation for loop-induced processes, JHEP **10** (2015) 146, [1507.00020].
[42] S. Baek, P. Ko and W. I. Park, Phys. Lett. B **747**, 255 (2015) doi:10.1016/j.physletb.2015.06.002 [arXiv:1407.6588 [hep-ph]].
[43] P. Ko, arXiv:1605.00061 [hep-ph].
[44] T. Sjostrand, S. Mrenna and P. Z. Skands, PYTHIA 6.4 Physics and Manual, JHEP **05** (2006) 026, [hep-ph/0603175].
[45] M. Cacciari, G. P. Salam and G. Soyez, The Anti-k(t) jet clustering algorithm, JHEP **04** (2008) 063, [0802.1189].
[46] M. Cacciari, G. P. Salam and G. Soyez, FastJet User Manual, Eur. Phys. J. **C72** (2012) 1896, [1111.6097].
[47] CMS collaboration, Search for dark matter in final states with an energetic jet, or a hadronically decaying W or Z boson using 12.9 fb^{-1} of data at $\sqrt{s} = 13$ TeV, Tech. Rep. CMS-PAS-EXO-16-037, CERN, Geneva, 2016.
[48] S. D. Ellis, C. K. Vermilion and J. R. Walsh, Recombination Algorithms and Jet Substructure: Pruning as a Tool for Heavy Particle Searches, Phys. Rev. **D81** (2010) 094023, [0912.0033].
[49] J. Thaler and K. Van Tilburg, Identifying Boosted Objects with N-subjettiness, JHEP **03** (2011) 015, [1011.2268].
[50] R. V. Harlander, S. Liebler and H. Mantler, SusHi: A program for the calculation of Higgs production in gluon fusion and bottom-quark annihilation in the Standard Model and the MSSM, Comput. Phys. Commun. **184** (2013) 1605–1617, [1212.3249].
[51] R. V. Harlander, S. Liebler and H. Mantler, SusHi Bento: Beyond NNLO and the heavy-top limit, 1605.03190.
[52] R. V. Harlander and W. B. Kilgore, Next-to-next-to-leading order Higgs production at hadron colliders, Phys. Rev. Lett. **88** (2002) 201801, [hep-ph/0201206].
[53] M. Cacciari, F. A. Dreyer, A. Karlberg, G. P. Salam and G. Zanderighi, Fully Differential Vector-Boson-Fusion Higgs Production at Next-to-Next-to-Leading Order, Phys. Rev. Lett. **115** (2015) 082002, [1506.02660].
[54] DELPHES 3 collaboration, J. de Favereau, C. Delaere, P. Demin, A. Giammanco, V. Lematre, A. Mertens et al., DELPHES 3, A modular framework for fast simulation of a generic collider experiment, JHEP **02** (2014) 057, [1307.6346].